Microscopic Dynamics Underlying the Broad Distribution of Stress Relaxation Times in Arrested Soft Materials

Jake Song,[1,2] Qingteng Zhang,[3] Felipe de Quesada,[1] Mehedi H. Rizvi,[4] Joseph B. Tracy,[4] Jan Ilavsky,[3] Suresh Narayanan,[3] Emanuela del Gado,[5] Robert L. Leheny,[6] Niels Holten-Andersen*[1] and Gareth H. McKinley*[2]

[1]*Department of Materials Science and Engineering and* [2]*Department of Mechanical Engineering, Massachusetts Institute of Technology*
[3]*X-ray Sciences Division, Argonne National Laboratory*
[4]*Department of Materials Science and Engineering, North Caroline State University*
[5]*Department of Physics, Georgetown University*
[6]*Department of Physics and Astronomy, Johns Hopkins University*
Corresponding emails: holten@mit.edu, gareth@mit.edu

Arrested soft materials such as gels and glasses exhibit a broad distribution of stress relaxation times in response to linear macro-rheological deformations. Although these relaxation dynamics play fundamental roles in the application of arrested systems as structural materials, consumer products, foods, and biological materials, the microscopic origins of such dynamics remains poorly understood. Here, we elucidate the microscopic dynamics that govern the stress relaxation of such arrested soft materials under both quiescent and mechanically-perturbed conditions through x-ray photon correlation spectroscopy. By studying the dynamics of a model associative gel system which undergoes dynamical arrest in the absence of aging effects, we show that the mean stress relaxation time measured from linear rheometry is directly correlated to the quiescent elastic fluctuations of the microscopic clusters which are governed by built-up internal stressses in the system. We also show that perturbing the system via small mechanical deformations can result in large intermittent fluctuations in the form of elastic avalanches, which give rise to a broad spectrum of non-Gaussian relaxation modes which are observed in stress relaxation measurements. These findings suggest that, even in the linear regime, stress relaxation in arrested soft materials may be a non-linear phenomenon which is governed by an interplay of internal stresses and perturbation-induced intermittent avalanches.

Keywords: soft materials, stress relaxation, avalanches, gels

A broad distribution of relaxation times in response to linear mechanical perturbations – manifested for instance via power-law or stretched-exponential stress relaxation curves – is recognized as a fundamental property in arrested soft materials, and occurs ubiquitously in glasses[1], concentrated emulsions,[2,3] gels,[4] surfactant solutions,[5] granular systems,[6] biological materials[7-11]. Despite this universality, the current understanding of this phenomenon is prevalently system-specific; for example, in glasses, non-exponential stress relaxations are approached from the perspective of dynamic heterogeneity,[1] referring to the spatiotemporal heterogeneities of mobilities that manifest within the glass microstructure[12]. In associative systems such as gels, stretched exponential stress relaxations are interpreted as a convoluted exponential relaxation process originating from an exponential or logarithmic distribution in the size of different relaxing mechanical components.[5,13,14] In strongly aging systems such as colloidal glasses and emulsions, relaxations are analyzed from the viewpoint of activated hops in an exponential potential energy landscape through a framework known as soft glassy rheology.[15,16] The quest to understand non-exponential stress relaxation in a variety of soft materials has also motivated studies of non-affine deformations,[17] non-linear internal prestress,[8] fractal structures,[18] shear-transformation zones,[19] aging induced avalanches,[3] interchain locking[20], and phase-separation.[21] This large variety of system-specific relaxation processes which have been proposed makes extracting the key physics behind broadly-distributed stress relaxation dynamics in arrested soft materials a complicated task.

Arrested soft materials also exhibit a common set of microscopic relaxation behaviors, manifested in the form of compressed exponential decay in the correlation functions and superdiffusive motion of the constituents.[22-26] The origins of these dynamics are well-understood as being athermal in nature, wherein internal stress heterogeneities generated during arrest are released and cause local strain propagation at a rate exceeding that from thermal rearrangements.[22-25,27,28] These microscopic dynamics are expected to play an important role in dictating the macroscopic relaxation dynamics of arrested systems. Indeed, evidence for this idea lies in past studies on gels[4] and biological networks,[11] where correlations between the aging-induced evolution of microscopic relaxation times and macroscopic relaxation times[4] or elastic moduli[11] have been established. However, despite these studies, a connection between the microscopic relaxation dynamics and the statistical features of the broad distribution of relaxation times in macroscopic perturbations (such as the mean and the width of the distribution of relaxation times) has remained elusive.

Significance Statement

The linear viscoelasticity of soft materials is governed by the microscopic thermal fluctuations of the underlying constituents of the system, which are expected to give rise to unique mono-exponential stress relaxation times. However, many soft materials such as glasses and gels instead exhibit a broad distribution of stress relaxation times, for which the microscopic origin remains elusive. Here, we investigate the microscopic fluctuations inside an arrested gel and reveal the presence of two distinct microscopic relaxation mechanisms – "quiescent" relaxations governed by the build-up of internal stresses during arrest, and "perturbation-induced" avalanche relaxation events governed by mechanical deformations in the system. We demonstrate that both relaxation mechanisms are essential components of non-exponential stress relaxations in arrested soft materials.

Here, we address this missing connection through a multi-scale investigation of the relaxation dynamics of an arrested model system via rheology, ultra-small-angle x-ray scattering, and x-ray photon correlation spectroscopy. The model system is a recently-developed associative hydrogel platform consisting of water-stabilized iron oxide nanoparticles (NPs),[29] which are bridged by telechelic linkers of 4-arm poly(ethylene glycol) (PEG) functionalized with strongly iron-coordinating nitrocatechol ligands (Fig. 1A). Prior work by our group,[30] as well as theoretical predictions on such gel systems,[31] have shown that this polymer-particle configuration facilitates dynamic arrest in the absence of a phase-separation[32] through limited-valency interactions. This mechanism of self-assembly results in gelation of the NPs via dynamic arrest, which allows the resulting gels to reach a structural and mechanical steady-state after gelation during the experimental timeframe rather than undergo continued aging via an arrested phase separation (Ref[30], Fig. S2), whilst still exhibiting hallmark behaviors of arrested soft materials such as stretched exponential stress relaxations and compressed exponential correlation decays.[30,33] This makes the limited-valency gel a useful model system for exploring the microscopic dynamics of arrested systems, as it eliminates the contribution of aging dynamics to microscopic relaxation dynamics[2,4,34]. and thus allow us to isolate the relaxation dynamics arising from perturbation-free quiescent states as well as in states under controlled external perturbation. Using this system, we are able to elucidate the separate contributions of dynamics arising from perturbation-free quiescent states and dynamics arising from perturbed states under controlled mechanical deformations, and evaluate their roles on the macroscopic stress relaxation of the system.

In response to a step strain in the linear regime, our arrested gel exhibits classic signatures of stretched exponential stress relaxations of the form:

$$G(t) = G_0 \exp(-(t/\tau_M)^{\beta}) \quad (1)$$

where G_0 is the plateau modulus, τ_M is the macroscopic relaxation time, and β is the stretching exponent. The gel shows an exponent of $\beta = 0.3$ across $25\,℃ < T \leq 65\,℃$ (Fig. 1B, S1). Stretched exponential stress relaxation functions underscore an asymmetric distribution in the relaxation times (with a mean relaxation time $\langle\tau\rangle$ and a heavy-tail at short times)[35], and are often seen in highly arrested systems such as gels and glasses.[1,4,5] We note that these relaxation dynamics are distinct from what is commonly seen (and well-understood) in associative gels at moderate concentrations of associations, wherein a power-law stress relaxation of $\sim t^{-1/2}$ emerges due to a "sticky" Rouse relaxation of interconnected components.[36,37] The arrest of interest here is clearly stronger, and typically appears in associative gels at high association strengths and concentrations.[38]

The microscopic dynamics of our model gel are measured via x-ray photon correlation spectroscopy (XPCS), a technique which allows us to directly measure the dynamics of the NP cross-linkers. XPCS bypasses the drawbacks of visible-light-based approaches in dealing with material opacity (Fig. 1B inset) and capitalizes on the high electron-density contrast between the NPs and the constituents (water and PEG). In XPCS, speckle intensity maps are measured as a function of time (Fig. 2A). The autocorrelation of the wave-vector q-dependent intensities produces a second-order correlation function $g_2(q,t)$ as a function of delay time t, which is related to the intermediate scattering function $F(q,t)$ via the Siegert relation:

$$g_2(q,t) = 1 + b[A\exp(-(t/\tau_m)^{\gamma}]^2 \quad (2)$$

where the front-factor $b \sim 0.1$ is an instrument-dependent coherence-adjustment factor, A is a contrast term, and τ_m and γ measure the microscopic relaxation time and associated stretching ($\gamma < 1$) or compressing ($\gamma > 1$) exponent of the decay curve (Fig. 2A). $F(q,t)$ is captured by the terms in the square brackets in Eqn. 2. More details on the technique are provided in reference.[39]

We perform XPCS over a q range of 0.0032 Å^{-1} to 0.063 Å^{-1}, which corresponds to the *intra-cluster* regime in our gel system (Fig. 2C). This intra-cluster regime is revealed by ultra-small-angle x-ray scattering (USAXS) measurements on the gels, through which contributions from three distinct length-scales are identified: a high-q contribution at $q \geq 1 \times 10^{-2}$ Å^{-1}; an intermediate-q contribution at 1×10^{-2} Å$^{-1} \leq q \leq 1 \times 10^{-2}$ Å^{-1}, and a low-q contribution at $q \leq 4 \times 10^{-3}$ Å^{-1}. The high-q contribution can be accurately modeled by a hard-sphere model (HSM) – the division of our intensity $I(q)$ by the HSM yields the structure factor $S(q)$, Fig. 2D – and can be attributed to the nanoparticles. The intermediate-q and low-q contributions can be attributed to the existence of clustering at multiple length-scales. These features are commonly observed in other network systems such as polymer gels[40] and nanocomposites through scattering measurements over large length-scales beyond the characteristic cluster size.[41] Here, we follow the conventions of these studies, and attribute the intermediate-q length-scale to primary clusters (cluster diameter $\xi = 3760$ Å via a unified model fit[42]) and the low-q length-scale to high-level agglomerates (with a characteristic diameter greater than the largest probed length-scale of USAXS, 1 μm, as evidenced by the Porod scaling of $I(q) \sim q^{-4}$). The XPCS region-of-interest thus falls within the primary cluster length-scale ξ.

We first probe the microscopic dynamics of the gel system in the quiescent state via XPCS using an *in situ* capillary-gelled sample (see Fig. S3 for holder setup). Second-order correlation $g_2(q,t)$ measurements on the capillary-gelled system reveal a compressed exponential decay, which is paired by superdiffusive dynamical behavior, as evidenced by the collapse of the $g_2(q,t)$ upon scaling the relaxation time τ_m by $q^{-\nu}$ (Fig. 2C). The scaling exponent $\nu \sim 1.07$ is obtained directly through the fitting of the mean value of $\tau_m(q)$ from 20 independent measurements (Fig. 2D); such ensemble-averaged measurements are only possible due to the negligible aging of the gelled material (Fig. S2). Within this same q region, the mean compressing exponent is $\gamma \sim 1.72$ (Fig. 2D) suggesting that superdiffusive dynamics persists throughout the intra-cluster length-scale. At high q, the relaxation time $\tau_m(q)$ deviates from this $q^{-\nu}$ scaling and γ decreases towards unity, in agreement with previous experiments[22] and simulations.[25] These observations are consistent with the aforementioned signatures of elastic stress fluctuations,[22-27] in which the relaxation of heterogeneous frozen-in internal stresses modifies the elastic strain field and induces superdiffusive local rearrangements in the material.

Though the heavy tail of the correlation decay is not fitted by the compressed exponential form of the Siegert relation in Fig. 2C (as also observed in many other compressed exponential decay measurements.[23,43,44]), we find a good collapse of the data in this tail region by $q^{-\nu}$, indicating that this heavy tail shares the same superdiffusive origins as the main decay function. We verify this, and directly shed light on the role played by internal stresses on the measured relaxation times τ_m, by performing an

azimuthal angle φ-dependent investigation of $g_2(q,t)$ in capillary-gelled systems. Capillary environments facilitate anisotropic residual stresses in the gels during dynamic arrest by preventing internal stress relaxations in the direction of boundary conditions such as the capillary walls and the sealant.[43] Thus, we would expect gel systems which relax via elastic fluctuations to exhibit a φ-dependence in the correlation decay, such that relaxation is accelerated in φ directions facing confinement. We indeed observe this behavior in our gels, where relaxation is faster along directions which are under confinement by the capillary walls and the Torr seal, and slower in unconfined directions (Fig. S3A-C). Internal stresses thus govern the measured relaxation times τ_m, as well as the distribution of relaxation events in the system which manifests as a heavy tail in the φ-averaged correlation data (Fig. 2C).

We now seek to establish a connection between the internal stress dominated microscopic relaxation time τ_m and statistical features of the broad distribution of relaxation times observed in macro-rhelogical experiments, namely the mean relaxation time $\langle\tau\rangle$ and the breadth of the distribution. The mean $\langle\tau\rangle$ of the distribution of relaxation times underlying a stretched exponential can be obtained by calculating the first moment of the stretched exponential function, via the relation[45]:

$$\langle\tau\rangle = (\tau/a)\Gamma(1/a) \tag{3}$$

where τ is the relaxation time and α is the generic exponent obtained from stretched exponentials, such as β in Eqn. 1 and γ in Eqn. 2.As the typical values obtained for exponents are vastly different between rheology and XPCS (stretched and compressed, respectively), we thus compare the mean rheological relaxation time $\langle\tau_M\rangle$, obtained by rescaling τ_M with β (Eqn. 1), with the mean XPCS relaxation time $\langle\tau_m\rangle$, obtained by rescaling τ_m with γ (Eqn. 2). We perform this comparison in a temperature-dependent manner, comparing τ_M obtained via rheology at $25\,℃ < T \leq 55\,℃$ with τ_m obtained via XPCS over the same temperature range. To enable this comparison, we study the correlation dynamics of our arrested system by gelling the system *ex situ* and gently loading it into an aluminum cell capable of conducting heat from the Peltier loaded in the XPCS chamber (Fig. S3). We underfill the cell to minimize perturbations to the sample. The microscopic dynamics lead to compressed-exponential correlation functions like those of the samples discussed above (see Fig. 4B), and hence we refer also to these samples as "quiescent".

Since $\langle\tau_m\rangle$ is q-dependent (Fig. 2D) and clearly smaller than $\langle\tau_M\rangle$ over the studied q-range (Fig. 3A), we select a specific characteristic microscopic length-scale at which the comparison with macroscopic measurements should be made. For this purpose, we choose the primary cluster size ξ as the characteristic length-scale, as cluster dynamics have often been implicated in dictating the macroscopic viscoelasticity of soft materials.[13,46-48] Scattering studies and simulations of arrested systems have shown that $\tau_m(q)$ may reach a plateau at wave-vectors larger than the cluster size q_ξ,[25,48,49] as microscopic dynamics become strongly constrained over such length-scales. These findings allow us to reliably extrapolate our superdiffusive scalings of $\tau_m \sim q^{-\nu}$ (as shown in Fig. 2D) down to the cluster-size wave-vector $q_\xi = 1/\xi = 2.7 \times 10^{-4}$ Å^{-1} to determine the characteristic relaxation times of the primary clusters of the gel, even if the q-range of XPCS does not explicitly capture such large length-scales.

The comparison between $\langle\tau_M(T)\rangle$ obtained via rheology with the $\langle\tau_m(q)\rangle$ obtained via XPCS are shown in Fig. 3A. Excellent agreements are observed between $\langle\tau_M(T)\rangle$ and the extrapolated quantity $\langle\tau_m(q_\xi,T)\rangle$, with $\langle\tau_m(q_\xi)\rangle/\langle\tau_M\rangle \sim 1$ for all temperatures studied (Fig. 3B). Representing the two quantities in an Arrhenius plot, we find that both measurements can be captured by a single Arrhenius function of the form $\langle\tau\rangle = \tau_0 \exp(-E_A/kT)$, with an activation energy $E_A \sim 21\,kT$ (Fig. 3C). The direct correlation between the mean macroscopic stress relaxation time and mean microscopic relaxation times at the cluster size shown here is rather striking, and indicates that internal stress relaxation of clusters at quiescence governs the mean macroscopic stress relaxation of the gel. This also indicates that stress relaxation in the gel is an inherently non-linear phenomenon, where the E_A represents the thermal activation energy of relaxation which is modified by internal stresses in the system.[50,51]

We next seek to understand the connection between microscopic dynamics and the breadth of stress relaxation times observed via linear rheology. Though we find that quiescent microscopic fluctuations are directly correlated to the mean macroscopic relaxation time of the system (Fig. 3), the distribution of τ_m is Gaussian, with a small variance which can be attributed to the spatial variation of the internal stresses in the microstructure (Fig. S5). This distribution of τ_m is not consistent with the broad distribution of relaxation times underlying a stretched exponential stress relaxation function with a stretching exponent as low as $\beta = 0.3$ (illustrated in Fig. S6). Thus, we reasoned that the macroscopic relaxation process may entail non-quiescent or perturbation-induced relaxation processes. Such pertubations, whether they originate from microstructural aging[3,52-54] or mechanical deformations[55] (even in the linear regime below the yield strain)[56] have been shown to induce avalanche dynamics in arrested systems, and recent simulation studies on emulsions have even hinted at a connection between avalanche dynamics and power-law macroscopic stress relaxation response through a microrheological framework.[3] As our quiescent systems show little structural and dynamical aging (Fig. S2) – especially within experimental timeframes (see two-time correlations of quiescent systems in Fig. S8) – we sought to induce such perturbations to our system through mechanical compressions. As an approximate approach to inducing such perturbations under XPCS, we again loaded a gel into the aluminum cell – the same approach as the one used to study temperature-dependent dynamics in Fig. 3 – but in this case overfilled the cell. Thus, in this state, the polycarbonate windows of the aluminum cell put the sample under a compressive strain of ___%, different from the quiescent samples that were underfilled in the cell (Fig. 4A).

A markedly different $g_2(t)$ response is observed in these perturbed systems compared to the quiescent systems (Fig. 4B). Whereas the quiescent systems exhibit a prototypical $g_2(q,t)$ which can almost be completely described by a single ballistic ($\sim \exp(-(t/\tau)^2)$ decay curve, the perturbed ones exhibit a much broader $g_2(t)$ which cannot be described by a single ballistic relaxation mode. To quantify these differences, we estimate the discrete spectra of ballistic relaxation modes governing the second-order correlation $g_2(q,t)$ of the quiescent and perturbed systems through an inverse Laplace transform of the relation:

$$g_2(t) = \int_{-\infty}^{\infty} H_m(\tau)[1 + \mathrm{b}(\mathrm{A}\exp(-t/\tau)^2)^2]d\ln\tau \tag{4}$$

where $H_m(\tau)$ is the spectrum of ballistic microscopic relaxation modes in the $g_2(t)$ functions. To perform this inverse Laplace transform, we use a non-linear regularization estimation[57] used commonly in macrorheology to determine $H_m(\tau)$; we find the discrete relaxation modes by identifying the dominant spectral peaks obtained by minimizing the curvature penalty in the regularization protocol (see Methods). Fig. 4C illustrates the results of this operation performed on the ensemble of dynamical data obtained on our arrested gels in quiescent and perturbed states. There is a marked difference in the breadth of the relaxation spectra of our system, shown by the emergence of short-time relaxation modes in the perturbed state which are absent in the quiescent state, but would be expected from a distribution of relaxation times underlying a stretched exponential with $\beta = 0.3$ (Fig. S6).

To understand the physics governing these emergent short-time dynamics in the perturbed system, we study the two-time correlations in the system, $C_I(t_1, t_2)$[39,44] (Fig. 5A, B; see Fig. S8 for larger ensemble of $C_I(t_1, t_2)$). The two-time correlation is a matrix representation of the instantaneous correlation of the system at measurement times t_1 and t_2, where the delay time $t = t_2 - t_1$(the correlation decay $g_2(q, t)$ is thus an ensemble average of the instantaneous correlations obtained by averaging over all pairs of measurement times of an experiment). For the quiescent configurations in the capillary and in the aluminum cell, we observe that the $C_I(t_1, t_2)$ bands are homogeneous across the measurement time (Fig. 5A). These observations indicate that the microscopic relaxation dynamics are temporally homogeneous over experimental timescales, and furthermore show the absence of dynamical processes at short times in the quiescent samples. However, with the introduction of mechanical perturbations, we observe highly intermittent correlation patterns with an abundance of narrowing in the bands, reminiscent of those seen in other disordered solids near the yielding transition (Fig. 5B).[58] These correlation patterns show that perturbation-induced intermittent dynamics give rise to the broadening in the relaxation spectrum through the emergence of short-time relaxation modes (Fig. 4C).

To quantify the statistical nature of these intermittent patterns, we compute the ensemble-averaged probability distribution function p of the two-time correlation $C_I(t_1, t_2)$ at different delay times. The instantaneous correlations in the quiescent state can be well-described by Gaussian distributions, consistent with the temporally homogeneous nature of the two-time correlation matrices (Fig. 5C). By contrast, the distribution of the instantaneous correlations in the perturbed state are highly non-Gaussian, and can be captured by a distribution which is commonly used for scale-free processes, namely the generalized Gumbel distribution:[59,60]

$$p(x) = \frac{a^a b_a}{\Gamma(a)} \exp\left(\mp a\left\{b_a(x+s_a) \pm \exp\left[-b_a(x+s_a)\right]\right\}\right) \quad (5)$$

where $b_a = \sqrt{d^2 \ln\Gamma(a)/da^2}\,/\sigma_x$, $s_a = \mu_x + \{\ln a - (d \ln\Gamma(a)/da)\}/b_a$. Here $\Gamma(a)$ is the Gamma function of a, μ_x and σ_x are the mean and standard deviations of x, and the $\mp$ and $\pm$ in Eqn 5. refers to the direction of the skew (such that – and + produce a heavy tail to the right, and vice versa). The shape parameter a in Eqn. 5 is given by the skewness or third moment of the distribution $\widetilde{\mu_3} = \langle[(x-\mu_x)/\sigma_x]^3\rangle \approx -1/\sqrt{a}$. This parameter a provides a measure of the distance to criticality in a given system,[61,62] where $a \to \infty$ for a Gaussian distribution, and $a \to 1$ in systems exhibiting scale-free dynamics and avalanches such as $1/f$ noise systems,[63] non-equilibrium colloidal gels[52,53], and glasses[64]. The distribution in the instantaneous correlation function of the perturbed system shows a pronounced Gumbel-like behavior at short times (Fig. 5D). This is quantified by the dependence of the shape parameter a as a function of the delay time t. At times shorter than the mean relaxation time of the system (i.e. $t < \langle\tau_m\rangle$), we see that $\alpha \to 1$ at all times (barring the sudden increase in the skewness at $t = 300$ s which naturally arises due to a skew direction change about the median time-scale of the avalanches).[53] At long times as the mean relaxation time of the system is approached (i.e. $t \sim \langle\tau_m\rangle$), α increases again and the system reverts to Gaussian statistics at long times (Fig. 5E). These results indicate that small mechanical perturbations generate avalanche-like fluctuations in the gel which persist at short times, before Gaussian fluctuations emerge at long times.

Thus, though microscopic internal stress relaxations in quiescent states exhibit strong correlations with the mean timescale of stress relaxation in arrested soft materials, we find that such quiescent dynamics do not explain the breadth of stress relaxation times observed in arrested systems via linear rheology. Instead, we find that these broadly distributed relaxation events – especially the broadening of the distributions towards shorter times, Fig. 4C, Fig. S6 – are observed at the microscopic scales in arrested systems which are perturbed, in our case through mechanical perturbations. Though these intermittent dynamics arise from a compressive strain that is ostensibly above the yield strain of the system (Fig. 1C), we postulate that the amount of strain in the system is not an important factor in triggering avalanche dynamics in the system. This is supported by the fact that the stress relaxation responses of the system are highly non-exponential across a wide range of magnitudes of step strain (Fig. 1C), regardless of the linearity of the strain – a dynamical response which only the non-Gaussian relaxation modes arising from perturbation-induced intermittent avalanches can account for. While avalanche dynamics have been understood to occur in arrested systems strained near or beyond the yield strain,[65,66] several recent works on dense amorphous materials such as metallic and colloidal glasess have shown that even small strains – well within the linear viscoelastic regime of the material – are sufficient for generating intermittent avalanches in the system.[55,56,67] Our findings thus provide insight into the important role played by such intermittent avalanches in the non-exponential macroscopic stress relaxations of arrested soft materials. These insights may have important ramifications for understanding the origins of non-exponential viscoelastic relaxations in a larger variety of soft materials, for instance biological hydrogels such as cells,[10] tissues,[9] and mucus[68].

Our work provides a connection between the microscopic relaxation dynamics of arrested systems, and the statistical features of the broad distribution of relaxation times in macroscopic mechanical measurements. We find that the quiescent superdiffusive microscopic dynamics of the gel at the cluster scale are governed by internal stress relaxations and show a direct correlation to the mean relaxation time measured via macro-rheology. We also find that perturbation-induced intermittent avalanche dynamics are necessary for attaining a broad non-Gaussian distribution of microscopic relaxation times in the system, thus rationalizing broad distribution of relaxation times observed in macro-rheological experiments. These promising findings warrant a quantitative investigation comparing

the microscopic relaxation modes arising from various rheologically-relevant perturbations with relaxation modes arising from microrheological measurements, a feat which may be possible via simulations as well as emerging experimental techniques such as Rheo-XPCS in conjunction with improved temporal resolution in coherent scattering from the planned advancements in synchrotron technology.[69,70] Results from such studies may provide insight into the quantitative physics underlying the extent of marginality and the manifestation of linear viscoelasticity in arrested materials.

Acknowledgements

We acknowledge funding from the National Science Foundation (CBET-1605943, CBET-1605699, CBET-1804721, DMR-1419807), the U.S. Army Research Office (through the Institute for Soldier Nanotechnologies under Contract No. W911NF-13-D-0001), and the U.S. Department of Energy (through the Argonne National Laboratory under Contract No. DE-AC02-06CH11357). J.S. would like to thank H. Le Roy, M. Lenz, T. Divoux, J.F. Douglas, J. H. Cho, I. Bischofberger, and J. Swan for helpful discussions.

Author Contributions

J.S. designed and executed the study under the supervision of N.H.A., and G.H.M. M.H.R and J.B.T synthesized nanoparticles. J.S., Q.Z., F.Q., and S.N performed XPCS experiments. J.S. and J.I performed USAXS experiments. E.D.G. and R.L.L, contributed to data interpretation. All authors contributed to the writing of the paper.

Competing Interest

The authors declare no competing interests.

References

1 Shang, B., Rottler, J., Guan, P. & Barrat, J.-L. Local versus global stretched mechanical response in a supercooled liquid near the glass transition. *Physical Review Letters* **122**, 105501 (2019).

2 Gopal, A. & Durian, D. J. Relaxing in foam. *Physical Review Letters* **91**, 188303 (2003).

3 Hwang, H. J., Riggleman, R. A. & Crocker, J. C. Understanding soft glassy materials using an energy landscape approach. *Nature Materials* **15**, 1031-1036 (2016).

4 Ramos, L. & Cipelletti, L. Ultraslow dynamics and stress relaxation in the aging of a soft glassy system. *Physical Review Letters* **87**, 245503 (2001).

5 Cates, M. & Candau, S. Statics and dynamics of worm-like surfactant micelles. *Journal Of Physics: Condensed Matter* **2**, 6869 (1990).

6 Brujić, J. *et al*. Granular dynamics in compaction and stress relaxation. *Physical Review Letters* **95**, 128001 (2005).

7 Holland, C., Terry, A., Porter, D. & Vollrath, F. Comparing the rheology of native spider and silkworm spinning dope. *Nature Materials* **5**, 870-874 (2006).

8 Mulla, Y., MacKintosh, F. & Koenderink, G. H. Origin of slow stress relaxation in the cytoskeleton. *Physical Review Letters* **122**, 218102 (2019).

9 Chaudhuri, O. *et al*. Hydrogels with tunable stress relaxation regulate stem cell fate and activity. *Nature Materials* **15**, 326 (2016).

10 Bursac, P. *et al*. Cytoskeletal remodelling and slow dynamics in the living cell. *Nature Materials* **4**, 557 (2005).

11 Lieleg, O., Kayser, J., Brambilla, G., Cipelletti, L. & Bausch, A. R. Slow dynamics and internal stress relaxation in bundled cytoskeletal networks. *Nature materials* **10**, 236-242 (2011).

12 Ballesta, P., Duri, A. & Cipelletti, L. Unexpected drop of dynamical heterogeneities in colloidal suspensions approaching the jamming transition. *Nature Physics* **4**, 550-554 (2008).

13 Douglas, J. F. & Hubbard, J. B. Semiempirical theory of relaxation: Concentrated polymer solution dynamics. *Macromolecules* **24**, 3163-3177 (1991).

14 Curro, J. G. & Pincus, P. A theoretical basis for viscoelastic relaxation of elastomers in the long-time limit. *Macromolecules* **16**, 559-562 (1983).

15 Sollich, P., Lequeux, F., Hébraud, P. & Cates, M. E. Rheology of soft glassy materials. *Physical Review Letters* **78**, 2020 (1997).

16 Fielding, S. M. Elastoviscoplastic rheology and aging in a simplified soft glassy constitutive model. *Journal Of Rheology* **64**, 723-738 (2020).

17 Liu, A. J., Ramaswamy, S., Mason, T., Gang, H. & Weitz, D. Anomalous viscous loss in emulsions. *Physical Review Letters* **76**, 3017 (1996).

18 Muthukumar, M. Screening effect on viscoelasticity near the gel point. *Macromolecules* **22**, 4656-4658 (1989).

19 Bouchbinder, E. & Langer, J. Linear response theory for hard and soft glassy materials. *Physical Review Letters* **106**, 148301 (2011).

20 Semenov, A., Charlot, A., Auzély-Velty, R. & Rinaudo, M. Rheological properties of binary associating polymers. *Rheologica Acta* **46**, 541-568 (2007).

21 Witten, T., Leibler, L. & Pincus, P. Stress relaxation in the lamellar copolymer mesophase. *Macromolecules* **23**, 824-829 (1990).

22 Duri, A. & Cipelletti, L. Length scale dependence of dynamical heterogeneity in a colloidal fractal gel. *Epl (Europhysics Letters)* **76**, 972 (2006).

23 Cipelletti, L. *et al*. Universal non-diffusive slow dynamics in aging soft matter. *Faraday Discussions* **123**, 237-251 (2003).

24 Ferrero, E. E., Martens, K. & Barrat, J.-L. Relaxation in yield stress systems through elastically interacting activated events. *Physical Review Letters* **113**, 248301 (2014).

25 Bouzid, M., Colombo, J., Barbosa, L. V. & Del Gado, E. Elastically driven intermittent microscopic dynamics in soft solids. *Nature Communications* **8**, 1-8 (2017).

26 Gnan, N. & Zaccarelli, E. The microscopic role of deformation in the dynamics of soft colloids. *Nature Physics* **15**, 683-688 (2019).

27 Srivastava, S. *et al*. Hyperdiffusive dynamics in newtonian nanoparticle fluids. *ACS Macro Letters* **4**, 1149-1153 (2015).

28 Bouchaud, J.-P. & Pitard, E. Anomalous dynamical light scattering in soft glassy gels. *The European Physical Journal E* **6**, 231-236 (2001).

29 Amstad, E., Gillich, T., Bilecka, I., Textor, M. & Reimhult, E. Ultrastable iron oxide nanoparticle colloidal suspensions using dispersants with catechol-derived anchor groups. *Nano Letters* **9**, 4042-4048 (2009).

30 Song, J. *et al*. Programmable Anisotropy and Percolation in Supramolecular Patchy Particle Gels. *ACS Nano* **14**, 17018-17027 (2020).

31 Lindquist, B. A., Jadrich, R. B., Milliron, D. J. & Truskett, T. M. On the formation of equilibrium gels via a macroscopic bond limitation. *The Journal Of Chemical Physics* **145**, 074906 (2016).

32 Zaccarelli, E. Colloidal gels: equilibrium and non-equilibrium routes. *Journal Of Physics: Condensed Matter* **19**, 323101 (2007).

33 Dudukovic, N. A. & Zukoski, C. F. Nanoscale dynamics and aging of fibrous peptide-based gels. *The Journal of Chemical Physics* **141**, 164905 (2014).

34 Pastore, R., Siviello, C., Greco, F. & Larobina, D. Anomalous Aging and Stress Relaxation in Macromolecular Physical Gels: The Case of Strontium Alginate. *Macromolecules* **53**, 649-657 (2020).

35 Lindsey, C. & Patterson, G. Detailed comparison of the Williams–Watts and Cole–Davidson functions. *The Journal Of Chemical Physics* **73**, 3348-3357 (1980).

36 Broedersz, C. P. *et al*. Cross-link-governed dynamics of biopolymer networks. *Physical Review Letters* **105**, 238101 (2010).

37 Chen, Q., Huang, C., Weiss, R. & Colby, R. H. Viscoelasticity of reversible gelation for ionomers. *Macromolecules* **48**, 1221-1230 (2015).

38 Chen, Q., Liang, S., Shiau, H.-S. & Colby, R. H. Linear viscoelastic and dielectric properties of phosphonium siloxane ionomers. *ACS Macro Letters* **2**, 970-974 (2013).

39 Leheny, R. L. XPCS: Nanoscale motion and rheology. *Current Opinion In Colloid & Interface Science* **17**, 3-12 (2012).

40 Matsunaga, T., Sakai, T., Akagi, Y., Chung, U.-i. & Shibayama, M. SANS and SLS studies on tetra-arm PEG gels in as-prepared and swollen states. *Macromolecules* **42**, 6245-6252 (2009).

41 Rishi, K. *et al*. Impact of an emergent hierarchical filler network on nanocomposite dynamics. *Macromolecules* **51**, 7893-7904 (2018).

42 Beaucage, G. Approximations leading to a unified exponential/power-law approach to small-angle scattering. *Journal Of Applied Crystallography* **28**, 717-728 (1995).

43 Dallari, F. *et al*. Microscopic pathways for stress relaxation in repulsive colloidal glasses. *Science Advances* **6**, eaaz2982 (2020).

44 Madsen, A., Leheny, R. L., Guo, H., Sprung, M. & Czakkel, O. Beyond simple exponential correlation functions and equilibrium dynamics in x-ray photon correlation spectroscopy. *New Journal Of Physics* **12**, 055001 (2010).

45 Guo, H. *et al*. Entanglement-controlled subdiffusion of nanoparticles within concentrated polymer solutions. *Physical Review Letters* **109**, 055901 (2012).

46 Whitaker, K. A. *et al*. Colloidal gel elasticity arises from the packing of locally glassy clusters. *Nature Communications* **10**, 1-8 (2019).

47 Cho, J. H., Cerbino, R. & Bischofberger, I. Emergence of Multiscale Dynamics in Colloidal Gels. *Physical Review Letters* **124**, 088005 (2020).

48 Krall, A. & Weitz, D. Internal dynamics and elasticity of fractal colloidal gels. *Physical Review Letters* **80**, 778 (1998).

49 Cipelletti, L., Manley, S., Ball, R. & Weitz, D. Universal aging features in the restructuring of fractal colloidal gels. *Physical Review Letters* **84**, 2275 (2000).

50 Nicolas, A., Ferrero, E. E., Martens, K. & Barrat, J.-L. Deformation and flow of amorphous solids: Insights from elastoplastic models. *Reviews Of Modern Physics* **90**, 045006 (2018).

51 Schall, P., Weitz, D. A. & Spaepen, F. Structural rearrangements that govern flow in colloidal glasses. *Science* **318**, 1895-1899 (2007).

52 Duri, A., Bissig, H., Trappe, V. & Cipelletti, L. Time-resolved-correlation measurements of temporally heterogeneous dynamics. *Physical Review E* **72**, 051401 (2005).

53 Filiberti, Z., Piazza, R. & Buzzaccaro, S. Multiscale relaxation in aging colloidal gels: From localized plastic events to system-spanning quakes. *Physical Review E* **100**, 042607 (2019).

54 Evenson, Z. *et al*. X-ray photon correlation spectroscopy reveals intermittent aging dynamics in a metallic glass. *Physical Review Letters* **115**, 175701 (2015).

55 Lin, J. & Wyart, M. Mean-field description of plastic flow in amorphous solids. *Physical Review X* **6**, 011005 (2016).

56 Shang, B., Guan, P. & Barrat, J.-L. Elastic avalanches reveal marginal behavior in amorphous solids. *Proceedings Of The National Academy Of Sciences* **117**, 86-92 (2020).

57 Honerkamp, J. & Weese, J. A nonlinear regularization method for the calculation of relaxation spectra. *Rheologica Acta* **32**, 65-73 (1993).

58 Das, A., Derlet, P. M., Liu, C., Dufresne, E. M. & Maaß, R. Stress breaks universal aging behavior in a metallic glass. *Nature Communications* **10**, 1-9 (2019).

59 Planet, R., Santucci, S. & Ortín, J. Avalanches and non-Gaussian fluctuations of the global velocity of imbibition fronts. *Physical Review Letters* **102**, 094502 (2009).

60 Barucci, A. *et al*. Universal fluctuations in tropospheric radar measurements. *Epl (Europhysics Letters)* **89**, 20006 (2010).

61 Joubaud, S., Petrosyan, A., Ciliberto, S. & Garnier, N. Experimental evidence of non-Gaussian fluctuations near a critical point. *Physical Review Letters* **100**, 180601 (2008).

62 Bertin, E. Global fluctuations and Gumbel statistics. *Physical Review Letters* **95**, 170601 (2005).

63 Antal, T., Droz, M., Györgyi, G. & Rácz, Z. 1/f noise and extreme value statistics. *Physical Review Letters* **87**, 240601 (2001).

64 Chamon, C., Charbonneau, P., Cugliandolo, L., Reichman, D. & Sellitto, M. Out-of-equilibrium dynamical fluctuations in glassy systems. *The Journal Of Chemical Physics* **121**, 10120-10137 (2004).

65 Lin, J., Lerner, E., Rosso, A. & Wyart, M. Scaling description of the yielding transition in soft amorphous solids at zero temperature. *Proceedings Of The National Academy Of Sciences* **111**, 14382-14387 (2014).

66 Budrikis, Z., Castellanos, D. F., Sandfeld, S., Zaiser, M. & Zapperi, S. Universal features of amorphous plasticity. *Nature Communications* **8**, 1-10 (2017).

67 Chen, Y., Rogers, S. A., Narayanan, S., Harden, J. L. & Leheny, R. L. Microscopic dynamics of stress relaxation in a nanocolloidal soft glass. *Physical Review Materials* **4**, 035602 (2020).

68 Wagner, C. E., Turner, B. S., Rubinstein, M., McKinley, G. H. & Ribbeck, K. A rheological study of the association and dynamics of MUC5AC gels. *Biomacromolecules* **18**, 3654-3664 (2017).

69 Leheny, R. L., Rogers, M. C., Chen, K., Narayanan, S. & Harden, J. L. Rheo-xpcs. *Current Opinion In Colloid & Interface Science* **20**, 261-271 (2015).

70 Borland, M. & Blednykh, A. The upgrade of the advanced photon source. (Brookhaven National Lab.(BNL), Upton, NY (United States), 2018).

Figures

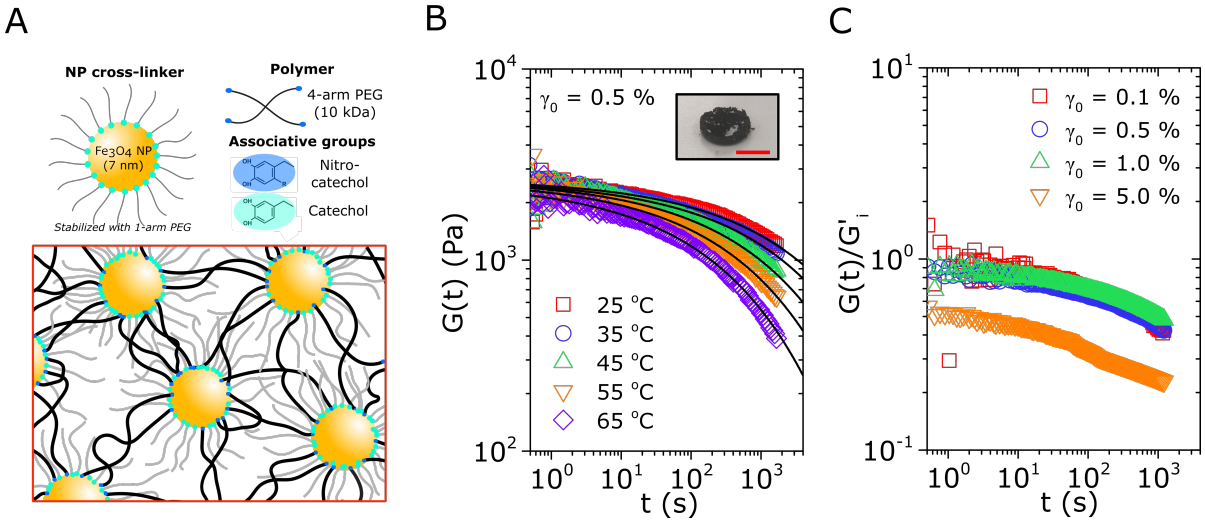

Figure 1. Arrested associative gels exhibit broad non-exponential stress relaxations in response to linear perturbations. A) Schematic illustration of the model polymer-particle system, consisting of 4-arm PEGs (10 kDa) with nitrocatechol groups, and Fe_3O_4 NPs (7 nm diameter) stabilized by 1-arm PEGs (2 kDa) with catechol groups. Upon mixing, the stronger-binding nitrocatechol ligand replaces the catechol ligand on the NP surface, and gelation thus occurs via a dynamic ligand exchange from equilibrium. Details on the synthesis and compositions are available in the Methods, and additional characterizations of the quiescent viscoelasticity of the gels are available in the reference.[25] B) Representative $G(t)$ of the arrested gel in response to a linear step strain ($\gamma_o = 0.5\%$) at $25℃ \leq T \leq 65℃$. Solid lines indicate fits to the stretched exponential function (Eqn. 1) with a constant value of $\beta = 0.3$. The stretching exponent is consistent at all temperatures, as evidenced by the stretched exponential fit to the time-temperature-superposed data (Figure S1). Inset: Representative picture of the model gel material, scale bar: 1 cm. C) Step strain measurements of the relaxation modulus $G(t)$ of the the gelled system measured at varying strain amplitudes γ_o ($T = 25^oC$). All $G(t)$ values are normalized by the initial storage modulus G_i' of the gel measured immediately after gelation (Fig. S2A). Linear behavior is demonstrated up to a strain of $\gamma_o = 1.0\%$; this result is also in agreement with amplitude sweep characterizations on the system (Fig. S2B).

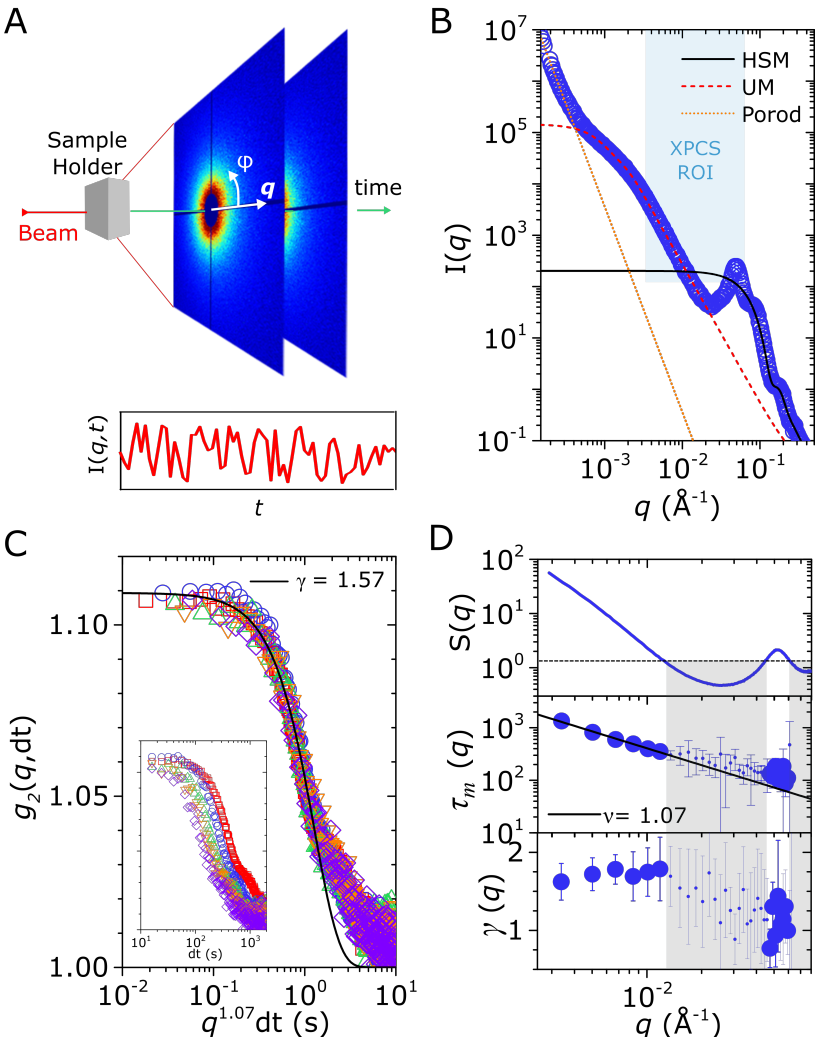

Figure 2. Microscopic dynamics of the arrested gel probed at quiescence via XPCS. A) Illustration of the XPCS experimental setup. A partially-coherent synchrotron x-ray beam strikes the sample, and scattered speckle intensity maps (with coordinates defined by the wave-vector q and azimuth angle ϕ) are measured as a function of time. Correlations of the measured speckle intensity $I(q,t)$ are taken to obtain the second-order correlation function $g_2(q,t)$ as a function of delay time t. B) Ultra-small-angle x-ray scattering (USAXS) intensities of the arrested gel. The scattering is captured by a hard-sphere model (HSM) at high q, a unified model (UM) at intermediate q, and a Porod scattering response at low q. The region-of-interest probed by XPCS is shown by the shaded region, which is bound by q = 0.0032 Å^{-1} and 0.063 Å^{-1} and a noise floor at low $I(q)$. The UM captures the cluster size ξ of the associative gel, and shows that the XPCS region-of-interest is within the primary cluster size. C) The second-order correlation function $g_2(q,t)$ as a function of delay time t for the arrested system *in situ* gelled in a capillary (see Fig. S3). The correlation decay is fitted to the Siegert relation in Eqn. 2. The x-axis is normalized by q^{ν} with $\nu = 1.07$; data collapse at indicates that the superdiffusive dynamics drives both the fitted decay and the long-time tail. D) q-dependent structure factor $S(q)$, microscopic relaxation time $\tau_m(q)$, and compressing exponent $\gamma(q)$. The $\tau_m(q)$ and $\gamma(q)$ values shown are averages taken from 20 independent experiments conducted in the SC1 geometry (see statistics in Fig. S5). The structure factor $S(q)$ is obtained by dividing $I(q)$ by the hard-sphere model results (Fig. 2B); dashed line in the $S(q)$ plot indicates the noise threshold dictated by low $I(q)$; measurements made at q corresponding to $S(q) < S(q)_{Noise}$ exhibit larger error bars as shown. The data points in this noise floor are indicated by smaller symbols, shaded in grey. The relaxation times above this noise floor, $\tau_m(q)$ at $q \leq 0.012$ Å^{-1}, are fitted to the relation $\tau_m(q) = Cq^{-\nu}$.

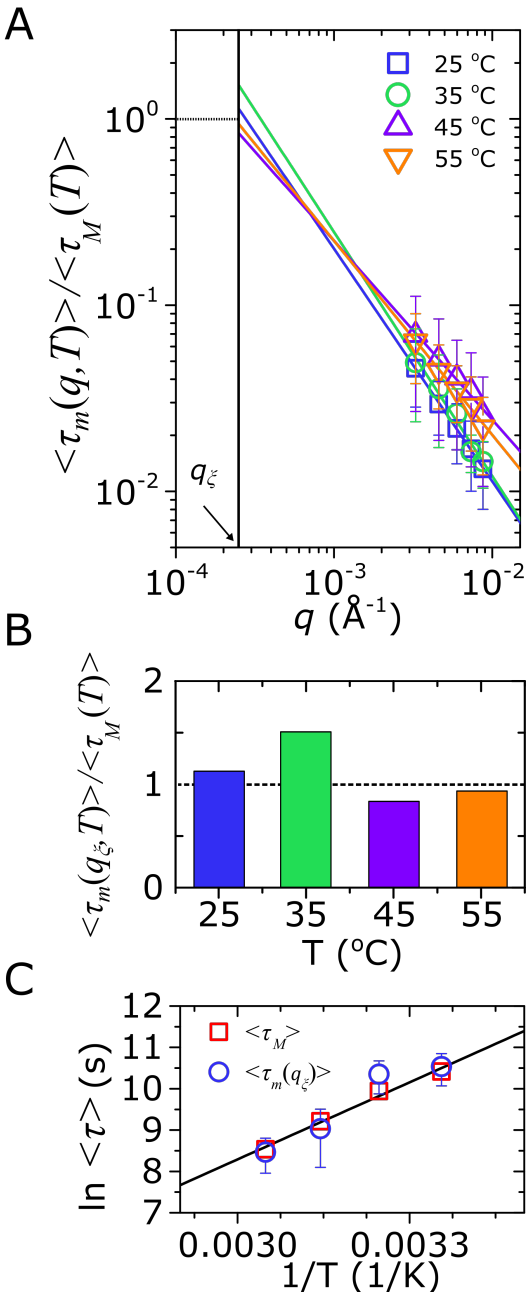

Figure 3. Correlations between quiescent microscopic cluster relaxation times and macroscopic stress relaxation times in the arrested gel. A) Mean microscopic relaxation times $\langle\tau_m(q,T)\rangle$ (see Eqn. 3) over a temperature range of $25^oC \leq T \leq 55^oC$ measured in an aluminum cell. All data are normalized to the mean macroscopic stress relaxation time at the corresponding temperatures $\langle\tau_M(T)\rangle$, fitted to the function $\langle\tau_m(q),T\rangle/\langle\tau_M(T)\rangle = Cq^{-\nu}$, and extrapolated to the wave-vector corresponding to the cluster size $q_\xi = 1/\xi = 2.7 \times 10^{-4}$ Å^{-1}. B) $\langle\tau_m(q_\xi,T)\rangle/\langle\tau_M(T)\rangle$ obtained via extrapolation to the cluster size. C) Arrhenius plot of the mean relaxation times obtained from rheology, $\langle\tau_M\rangle$, and from XPCS, $\langle\tau_m(q_\xi)\rangle$. Lines indicate fits of $\langle\tau_M\rangle$ to the Arrhenius relation $\langle\tau\rangle = \tau_0 \exp(-E_A/kT)$, which reliably captures $\langle\tau_m(q_\xi)\rangle$ as well. Fitting parameters in Tables S2 and S3.

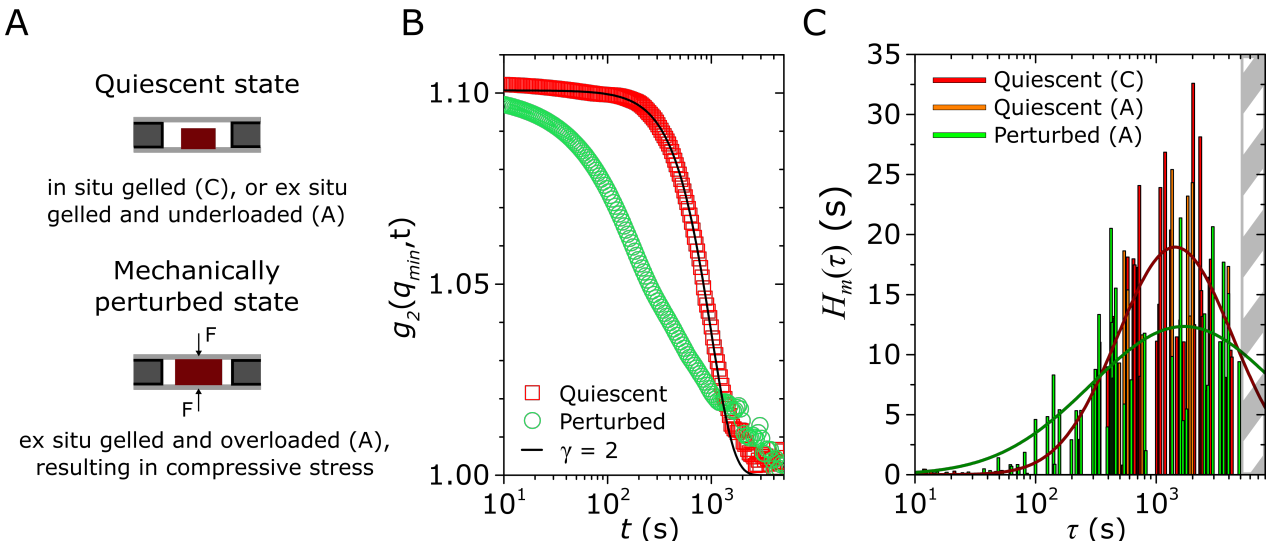

Figure 4. Perturbation-induced broadening of the distribution of microscopic relaxation times in the arrested gel. A) Configurational descriptions of the gel system which are in quiescent states and mechanically perturbed states. The quiescent states are probed either through *in situ* gelation of the system in a capillary (denoted C), or through underloading an aluminum cell (denoted A) with an *ex situ* gelled material. Detailed illustration of the C and A configurations are in Fig. S3. We induce mechanical perturbations to our gels by overloading the aluminum cell with the *ex situ* gelled material, resulting in compressive stress. B) Representative second-order correlations g_2 at $q_{min} = 0.0032$ Å^{-1} for the quiescent system (in capillary) and perturbed system. Here, higher q data are horizontally shifted (in similar vein to Fig. 2C) to access longer time-scales of $t \sim 4000$ s. The quiescent system in the aluminum cell shows a similar response to that in the capillary (data not shown). The quiescent data shows good agreement with Eqn. 2 with a ballistic decay exponent of $\gamma = 2$. C) Discrete spectra of ballistic microscopic relaxation times $H_m(\tau)$ in the quiescent and perturbed systems at $q_{min} = 0.0032$ Å^{-1} and $T = 25^oC$, obtained via Eqn. 4. The analysis is done on 15 experiments in the capillary configuration, 6 experiments in the aluminum configuration at quiescence, and 11 experiments in the aluminum configuration under perturbations. The vertical shading at $t > 4000\ s$ denotes the time-scale limitations of the experiments (see Fig. 4B). The quiescent data (capillary and aluminum cell data combined) and perturbed data are fitted to a Gaussian function of the form $H_m(\tau) = k \exp\left(-\frac{(x-b)^2}{2c^2}\right)$ (red and green lines, respectively). Note the fits are for visual guidance only to highlight the emergence of short-time dynamics in the perturbed system.

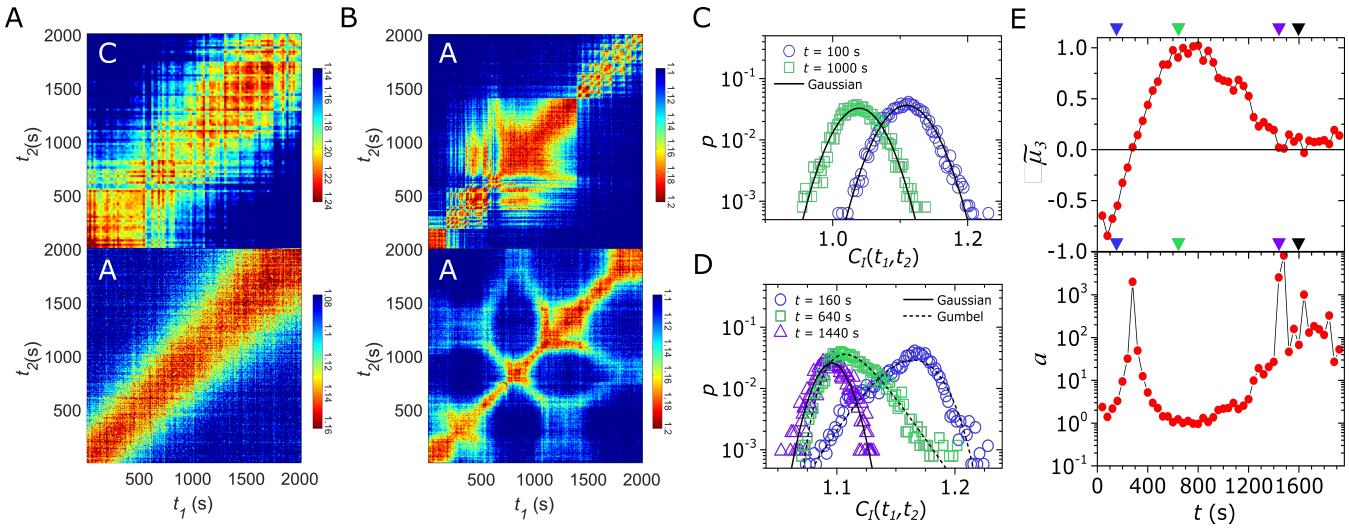

Figure 5. Avalanche statistics of the emergent short time dynamics in the mechanically perturbed gel. Representative two-time intensity correlation functions C_I of the arrested gel in the A) quiescent state (top: capillary, bottom: aluminum cell) and B) mechanically perturbed state (aluminum cell) at $q = 0.0032$ Å^{-1} (see Figure S4 for a larger ensemble of data). Probability distribution function p of the two-time correlation C_I at the indicated delay times at $q = 0.0032$ Å^{-1} for the arrested gel at C) quiescent states (capillary) across 20 experiments, and D) perturbed states across 15 experiments. The instantaneous correlation fluctuations are Gaussian for the quiescent samples at all delay times probed, whereas the perturbed samples exhibit highly non-Gaussian fluctuations at short times which are captured by a generalized Gumbel distribution (Eqn. 5) before reverting to Gaussian statistics near the microscopic relaxation time τ_m. The generalized Gumbel distributions shown (dashed lines) are calculated numerically by calculating the skewness parameter a directly from the data (via the third moment $\widetilde{\mu_3}$, where $1/\sqrt{a} = -\widetilde{\mu_3}$), rather than fitted. E) Third moment $\widetilde{\mu_3}$ of the correlation fluctuations and the corresponding skewness parameter a as a function of t for the perturbed system. Colored triangles indicate delay times t corresponding to those shown in D); black triangles indicate the quiescent relaxation time τ_m at $q = 0.0032$ Å^{-1} (Fig. 2D).